Debye-Waller factor in solid ^{3}He and ^{4}He

E. W. Draeger and D. M. Ceperley
Department of Physics and National Center for Supercomputing Applications, University of Illinois, Urbana-Champaign, Illinois 61801
(Received 14 October 1999)

The Debye-Waller factor and the mean-squared displacement from lattice sites for solid ^{3}He and ^{4}He were calculated with path-integral Monte Carlo at temperatures between 5 and 35 K, and densities between 38 and 67 nm^{-3}. It was found that the mean-squared displacement exhibits finite-size scaling consistent with a crossover between the quantum and classical limits of $N^{-2/3}$ and $N^{-1/3}$, respectively. The temperature dependence appears to be T^3, different than expected from harmonic theory. An anisotropic k^4 term was also observed in the Debye-Waller factor, indicating the presence of non-Gaussian corrections to the density distribution around lattice sites. Our results, extrapolated to the thermodynamic limit, agree well with recent values from scattering experiments.

I. INTRODUCTION

Solid helium at low temperatures is the prototype quantum crystal[1], since its ground state is not well described by harmonic perturbations about a minimum potential configuration. For temperatures between 5 and 35 K, and densities between 38 and 67 nm^{-3}, the kinetic energy is always greater than about 25 K and dominates over thermal energies. Solid helium has a wide range of experimentally accessible temperatures and densities. With new scattering sources, the density distribution and other correlation functions can be measured with unprecedented accuracy, allowing for a careful comparison between theory and experiment.

It is possible to calculate the properties of helium very accurately using Monte Carlo methods, because the interatomic potential is accurately known, more accurately than any other atomic or molecular condensed matter system. Additionally, for bosonic and distinguishable particle systems, path-integral Monte Carlo (PIMC) methods can calculate equilibrium properties directly from an assumed Hamiltonian without significant approximation. Even in the case of solid ^{3}He, effects of Fermi statistics can be neglected for temperatures above 0.1 K and densities slightly away from melting.

In scattering, the Debye-Waller factor is the fractional intensity shift due to recoilless processes, and can be directly related to the one-dimensional mean-squared displacement of particles from their lattice sites $\langle u^2\rangle$. In this paper we compute $\langle u^2\rangle$ and compare it to experimental results, obtaining good agreement. In the process we make several interesting observations. First, the density distribution of helium atoms is slightly non-Gaussian, a fact that had been speculated on but not yet observed. Second, we observe some unusual dependence of $\langle u^2\rangle$ on the size of the finite system being simulated, indicating a scaling crossover between the quantum and classical regimes. The dependence of $\langle u^2\rangle$ on the number of atoms N being simulated appears to be well-described by harmonic theory. Finally, the temperature dependence appears to be T^3, rather than the T^2 predicted by harmonic theory.

A. Debye-Waller Factor

The static structure factor, as measured in scattering, is defined as

$$S(k)=\langle|\rho_k|^2\rangle, \tag{1}$$

where $\rho_k\equiv(1/\sqrt{N})\Sigma_i e^{i\mathbf{k}\cdot\mathbf{r_i}}$. The structure factor can be computed directly with PIMC for finite systems of $N\lesssim 10\,000$ atoms. In a solid, the structure factor has large peaks at the reciprocal-lattice vectors of the perfect lattice. It is usually assumed that the magnitude of $S(k)$ behaves as

$$S(k)\propto\exp(-2W)\cong\exp(-k^2\langle u^2\rangle), \tag{2}$$

where $\exp(-2W)$ is the Debye-Waller factor. This equation relies on the assumption that the particle densities are normally distributed about the lattice sites.

We will now derive a more general form of Eq. (2). We will assume a finite system, with periodic boundary conditions and precisely N particles at positions $\mathbf{r}_i$ and N perfect lattice sites $\mathbf{Z}_i$. Using particle symmetry, we can rewrite Eq. (1) as

$$S(k)=1+(N-1)\langle e^{i\mathbf{k}\cdot(\mathbf{r_1}-\mathbf{r_j})}\rangle_j, \tag{3}$$

where the angle brackets $\langle\rangle_j$ denote an average over both the thermal density matrix *and* particles $j\neq 1$. When $\mathbf{k}$ is a reciprocal-lattice vector,

$$e^{i\mathbf{k}\cdot(\mathbf{r_1}-\mathbf{r_j})}=e^{ik(u_1-u_j)}, \tag{4}$$

where $u_i=\hat{\mathbf{k}}\cdot(\mathbf{r_i}-\mathbf{Z_i})$ is the displacement of particle i from its lattice site in the direction of $\mathbf{k}$. We assume a simple Bravais lattice, and assign each particle to a lattice site. Now consider the variable $x\equiv u_1-u_j$. Using the cumulant expansion[2] to evaluate the average of an exponential in terms of the moments of x, we can write

$$\langle e^{ikx}\rangle=\exp\left(-\frac{k^2}{2}\langle x^2\rangle+\frac{k^4}{24}(\langle x^4\rangle-3\langle x^2\rangle^2)+\cdots\right), \tag{5}$$

since the odd powers of x in the expansion vanish under the interchange $1\leftrightarrow j$ allowed by particle symmetry. For a system much larger than the correlation length ξ of u, which is finite in solid helium, u_1 is uncorrelated with u_j except for the neighbors of particle 1. Hence

$$\langle x^2\rangle = 2\langle u^2\rangle - 2\langle u_1 u_j\rangle \cong 2\langle u^2\rangle + \mathcal{O}[(\xi/L)^3],$$

$$\langle x^4\rangle = 2\langle u^4\rangle + 6\langle u^2\rangle^2 - 4\langle u_1^3 u_j\rangle - 4\langle u_1 u_j^3\rangle$$
$$\cong 2\langle u^4\rangle + 6\langle u^2\rangle^2 + \mathcal{O}[(\xi/L)^3]. \tag{6}$$

Here, L is the box length. Combining Eqs. (3), (5), and (6), we obtain

$$S(k) \cong 1 + (N-1)\exp\left(-k^2\langle u^2\rangle + \frac{\kappa k^4}{12}\langle u^2\rangle^2\right), \tag{7}$$

where the kurtosis κ is defined as the relative deviation of the fourth moment from a normal distribution,

$$\kappa \equiv \frac{\langle u^4\rangle}{\langle u^2\rangle^2} - 3. \tag{8}$$

The kurtosis vanishes if the density distribution is normal in the scattering direction. Previous analysis of this kind has assumed Gaussian fluctuations, and hence neglected all higher-order terms beyond the first. However, we find that the kurtosis is not precisely zero and has directional dependence.

The directional dependence is constrained by the crystal symmetry. From Eqs. (5) and (6), it follows that

$$\langle(\mathbf{k}\cdot\mathbf{u})^2\rangle = \sum_{\alpha,\beta} k_\alpha k_\beta S^{(2)}_{\alpha\beta}, \tag{9}$$

$$\langle(\mathbf{k}\cdot\mathbf{u})^4\rangle = \sum_{\alpha,\beta,\gamma,\delta} k_\alpha k_\beta k_\gamma k_\delta S^{(4)}_{\alpha\beta\gamma\delta} \tag{10}$$

where $S^{(2)}$, $S^{(4)}$ are tensors, completely symmetric in their indices. For a Bravais lattice with inversion symmetry the only nonzero elements are ones with pairs of repeated indices. Then, because of cubic symmetry, $S^{(2)}_{\alpha\beta} = \langle u^2\rangle\delta_{\alpha\beta}$ and $S^{(4)}_{\alpha\beta\gamma\delta}$ has only two independent elements S_{xxyy} and S_{xxxx}. We can determine these elements by fitting the kurtosis along different crystal axes. We choose κ_{100} and κ_{111} for fcc. The spherically averaged kurtosis is given by

$$\bar{\kappa} \equiv 3\left[\frac{\langle r^4\rangle}{15\langle u^2\rangle^2} - 1\right]$$
$$= \frac{3}{5}\kappa_{111} + \frac{2}{5}\kappa_{100}. \tag{11}$$

II. PIMC CALCULATIONS OF SOLID HELIUM

Path-integral Monte Carlo simulations were performed as discussed in Ref. 3. The system being simulated consists of particles (boltzmannons) in a box with periodic boundary conditions at a fixed density. Approximating the particles as boltzmannons should be valid as long as there are no vacancies and the temperature is greater than the exchange frequency $\cong 10^{-6}$ K (see Table II, Ref. 3). The helium atoms were assumed to interact pairwise with the Aziz potential[4]. Although small errors in energy are expected with this potential due to the absence of three-body interactions, we expect the pair potential to describe well the density distribution due to the fact that three-body and higher-order contributions are smoothly varying with respect to atomic positions. Although newer pair potentials now exist,[5,6] we believe the Aziz potential to be sufficiently accurate for these calculations. We implicitly test these assumptions by comparing to experimental values. The pair potential was set to zero for interatomic distances greater than 6 Å. We determined that this is the minimum cutoff that could be used without causing systematic errors in the mean-squared displacement. The pair potential was used to compute the exact pair density matrix for the system with an imaginary time step equal to $\tau = 1/160$ K^{-1}. Using this action, the time step error was found to be negligible. We used neighbor lists to achieve linear scaling of the computer time versus the number of atoms, and were able to simulate systems of up to 3000 atoms. Typically, about 50 000 Monte Carlo passes were used.

We computed the Debye-Waller factor two different ways. First, $\langle u^2\rangle$ was computed directly from the distance of the atoms from their lattice sites,

$$\langle u^2\rangle = \frac{1}{3}\left\langle \frac{1}{NM}\sum_{i=1}^{N}\sum_{j=1}^{M}(\mathbf{r}_{ij} - \mathbf{Z}_i)^2\right\rangle, \tag{12}$$

where M is the number of imaginary time slices, N is the number of particles, and $\mathbf{r}_{ij}$ is the position of particle i at imaginary time slice j. The factor of 1/3 arises because in a cubic crystal we can also average over the three spatial directions.

For the sake of convenience, it is useful to forbid particle exchanges between lattice sites so that the particles do not have to be periodically reassigned to the nearest site. We assured localization to a lattice site by ''tethering'' each particle: specifying a distance from its lattice site past which all attempted moves were rejected. The tether distance, 2.6 Å, was chosen to be on the order of, but slightly less than, the average nearest-neighbor distance and did not introduce a noticeable change in $\langle u^2\rangle$ or the structure factor.

The second method for computing the Debye-Waller factor was to calculate $S(k)$ directly from Eq. (1) from the set of all reciprocal-lattice vectors of $k \leqslant 9$ Å^{-1} and then use Eq. (7) to determine $\langle u^2\rangle$ and the kurtosis κ by a least-squares fit to $\ln[(S(k)-1)/(N-1)]$. This method has the advantage of not requiring tethering or indeed any of the assumptions used in deriving Eq. (7). It also allows one to determine not only $\langle u^2\rangle$ but also any non-Gaussian components. Agreement between the two approaches shows that correlations in u in Eq. (6) do decay rapidly. Calculating $\langle u^2\rangle$ either directly with Eq. (12) or from fitting to $S(k)$ always gave the same value within statistical error, with similar error bars (see Fig. 1).

III. FINITE-SIZE SCALING

Before we can present the comparison to experiment, we must extrapolate the results obtained for a finite system to the thermodynamic limit. We observed a very slow convergence. To carefully examine the finite-size effects we simulated much larger systems (up to 3000 atoms) than had been done previously with PIMC. Even with the increased range of system size, the finite-size effects are not well described by a power law, but are instead in a crossover region. For the temperature and density values studied in this paper, the

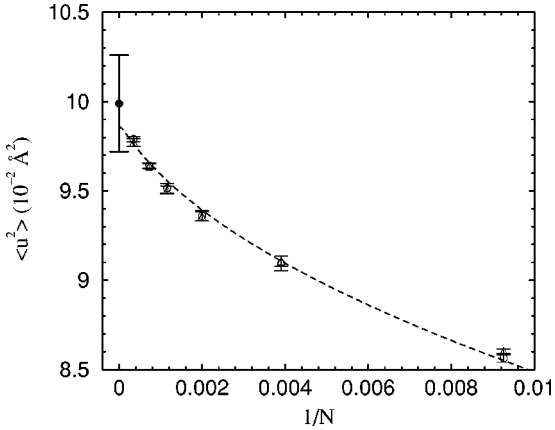

FIG. 1. Extrapolation of finite PIMC simulation data to the thermodynamic limit, for fcc ^{4}He, $V_m = 10.98$ cm^3, $T = 20.0$ K. $\langle u^2 \rangle$ was calculated by direct averaging (open circles) and by fitting to $S(k)$ data (open triangles). Both methods always agreed within statistical error bars. Least-squares fitting was used to fit the directly averaged data to Eq. (23). The experimental data point (solid circle) is from Arms and Simmons.

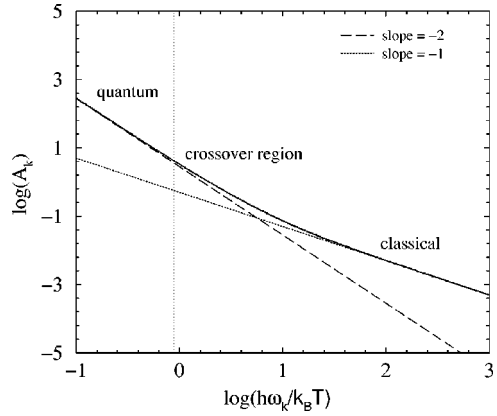

FIG. 2. Numerical calculation of $A(k)$ as a function of $\hbar\omega_k/k_BT$, for a damped harmonic oscillator with linewidth $\gamma_k = 0.2\omega_k$. Shown is the crossover between the quantum limit (dashed line) and the classical limit (dotted line), which allows one to estimate the range of system sizes affected by the crossover region.

crossover region appears to span the range of system sizes available to present computer simulation ($N_{\text{crossover}} \leqslant 10^5$), requiring careful fitting to obtain values in the thermodynamic limit.

Young and Alder[7] have used Debye theory to analyze the finite-size dependence of a system of classical hard spheres and determined that $\langle u^2 \rangle \propto \rho^{-2/3} T N^{-1/3}$. They found that this scaling was accurately able to fit values obtained with molecular-dynamics simulations. Recent classical Monte Carlo calculation on a Lennard-Jones model of an fcc solid[8] also found the same dependence.

Runge and Chester[9] looked at the size effects of a hard-sphere system using PIMC. Using the same Debye theory but now taking quantum effects into account, they estimated that the finite-size effects scale as $N^{-2/3}$ at zero temperature, and found a crossover from the quantum to the classical scaling ($N^{-1/3}$) as the temperature was increased.

MacFarland *et al.*[10] used shadow wave functions at $T=0$ to compute the finite-size scaling of the Debye-Waller factor for solid ^{4}He. However, these calculations neglected the effects of long-range correlations in the wave function induced by phonons, which are implicitly included in PIMC. Because of the neglect of these phonons, they found classical finite-size scaling proportional to $N^{-1/3}$.

We used harmonic theory to derive a reasonable functional form for the finite-size effects of $\langle u^2 \rangle$ in a crossover region and the width of that crossover region. In general, one can write the mean-squared displacement as[11]

$$\langle u^2 \rangle = a^3 \int \frac{d^3\mathbf{k}}{(2\pi)^3} \int \frac{d\omega}{2\pi} \frac{A(\mathbf{k},\omega)}{e^{\beta\hbar\omega}-1}, \tag{13}$$

where $A(\mathbf{k},\omega)$ is the spectral function for the displacement-displacement Green's function, $a^3 = 1/\rho$ is the volume of the unit cell, and $\beta = 1/k_BT$. It is useful to define

$$A(\mathbf{k}) = \int_{-\infty}^{\infty} \frac{d\omega}{2\pi} \frac{A(\mathbf{k},\omega)}{e^{\beta\hbar\omega}-1} \tag{14}$$

so that

$$\langle u^2 \rangle = \frac{a^3}{(2\pi)^3} \int d^3\mathbf{k} A(\mathbf{k}). \tag{15}$$

Let us assume that the effect of the periodic boundary conditions is to replace the integral in Eq. (13) with a sum

$$\delta\langle u^2 \rangle \equiv \langle u^2 \rangle_\infty - \langle u^2 \rangle_N = \frac{a^3}{(2\pi)^3} \int d^3\mathbf{k} A(\mathbf{k}) - \frac{a^3}{(2\pi)^3} \sum_{\mathbf{k}\neq 0} A(\mathbf{k}) k_c^3. \tag{16}$$

The finite spacing of $\mathbf{k}$ is a function of the system size, and is given by $k_c = 2\pi(\rho/N)^{1/3}$ for a cubic simulation cell. The main contribution to the finite-size error is due to the omission of the $\mathbf{k}=0$ value. If we further assume that for small values of k that $A(\mathbf{k})$ factors into an analytic function (smooth and continuous near $k=0$) and a singular factor $|k|^{-\nu}$, then it can be shown that the dominant term in Eq. (16) is

$$\delta\langle u^2 \rangle \propto k_c^{3-\nu} \propto N^{(\nu/3)-1}. \tag{17}$$

According to this theory, one must determine the exponent ν of the singular part of the Green's function $A(k)$, at $k=0$.

For a harmonic lattice,

$$A_{\text{harmonic}}(\mathbf{k},\omega) = \frac{2\pi\hbar}{2m\omega_k}[\delta(\omega-\omega_k) - \delta(\omega+\omega_k)], \tag{18}$$

where ω_k is the frequency of a phonon of wave vector k and m is the mass. In the limit of small k, the dispersion ω_k is linear in k. Integrating over ω, we obtain

$$A(k) = \frac{\hbar}{m} \frac{1}{\omega_k} \coth\left(\frac{\beta\hbar\omega_k}{2}\right). \tag{19}$$

Thus for $k_BT \gg \hbar\omega_k$ we find $\nu=2$, but at $T\approx 0$, $\nu=1$, as did Young and Alder[7] and Runge and Chester.[9] A crossover between the two scaling forms occurs at $\hbar\omega_k \approx k_BT$.

TABLE I. PIMC results. $\langle u^2\rangle_\infty$ was estimated by fitting finite PIMC data to the function given in Eq. (23), assuming a sound speed $s=4000\pm2000$ m/sec. The listed uncertainty in $\langle u^2\rangle_\infty$ represents the range of fitted values corresponding to the uncertainty in s. The errors in the energies represent the statistical uncertainties in the final digit, while the experimental errors are the total uncertainties as estimated by the authors. κ_{100} represents the estimated kurtosis in the $\langle 100\rangle$ direction. κ was estimated for the largest system size available, usually $N=1372$.

Type	V_m(cm^3)	T (K)	$T_{\rm expt}$ (K)	$\langle u^2\rangle_\infty$($10^{-2}$ Å^2)	$\langle u^2\rangle_{\rm expt}$($10^{-2}$ Å^2)	κ_{100}	$E_{\rm kinetic}$ (K)	$E_{\rm tot}$ (K)
fcc ^{4}He	10.98	20.00	20.25	9.77(39)	9.99(27) [a]	0.09	80.30(2)	50.24(2)
fcc ^{4}He	10.98	17.78		9.15(32)		0.08	79.10(4)	48.02(5)
fcc ^{4}He	10.98	16.84		8.71(23)		0.07	79.15(6)	47.52(6)
fcc ^{4}He	10.98	16.00		8.76(21)		0.07	78.51(4)	46.64(4)
fcc ^{4}He	10.98	15.24		8.49(18)		0.06	78.61(6)	46.44(6)
fcc ^{4}He	10.98	13.33		8.36(16)		0.06	77.63(4)	45.08(4)
fcc ^{4}He	10.98	10.00		8.02(8)		0.06	77.06(2)	43.99(2)
fcc ^{4}He	10.98	8.00		7.89(7)		0.06	76.87(4)	43.67(3)
fcc ^{4}He	10.98	5.00		7.79(5)		0.06	76.80(2)	43.50(2)
fcc ^{4}He	10.39	24.60	24.40	8.89(53)	8.23(40) [b]	0.09	90.41(4)	68.71(5)
fcc ^{4}He	10.02	26.67	25.94	8.29(61)	8.43(18) [b]	0.09	96.48(4)	81.53(4)
fcc ^{4}He	9.02	35.56	38.00	6.91(94)	5.66 [c]	0.09	118.14(7)	133.74(8)
fcc ^{4}He	9.02	22.86		5.77(21)		0.04	110.68(5)	120.77(5)
fcc ^{4}He	9.43	21.33		6.31(21)		0.05	109.14(6)	114.16(6)
fcc ^{4}He	9.97	26.67	28.00	8.14(58)	6.93 [c]	0.08	101.33(5)	94.26(5)
fcc ^{4}He	9.97	18.82	19.00	7.04(20)	6.20 [c]	0.05	98.82(6)	88.03(6)
fcc ^{3}He	11.54	17.78	18.13	11.41(40)	11.43(11) [a]	0.10	86.14(3)	58.53(3)
fcc ^{3}He	11.54	10.00		10.00(12)		0.08	84.15(4)	54.68(4)
fcc ^{3}He	11.54	5.00		9.72(5)		0.12	83.88(5)	54.22(4)
fcc ^{3}He	10.98	17.78		9.87(28)		0.09	93.18(5)	70.39(5)
fcc ^{3}He	10.00	29.09		9.07(76)		0.09	113.74(5)	110.00(6)
hcp ^{4}He	12.12	14.55	14.23	11.17(13)	11.25(28) [a]		66.44(4)	27.95(4)
hcp ^{4}He	12.12	11.85	12.00	10.24(13)	10.26(17) [a]		65.56(6)	26.16(6)
hcp ^{4}He	12.12	5.00		9.52(5)			64.37(3)	24.15(3)
hcp ^{4}He	15.72	5.71	5.80	17.40(13) [d]	17.31(18) [e]		40.66(3)	0.78(3)
hcp ^{4}He	10.98	5.00		7.78(3)			76.74(4)	43.47(3)
hcp ^{3}He	11.90	16.84	16.81	11.84(24)	11.96(26) [a]		82.17(6)	52.13(6)
hcp ^{3}He	12.81	12.31	12.54	13.26(19)	13.43(27) [a]		71.14(4)	36.37(4)

[a]Arms and Simmons (Ref. 15). Direct x-ray measurements.
[b]Venkataraman and Simmons (Ref. 16). Direct x-ray measurements.
[c]Thomlinson, Eckert, and Shirane (Ref. 17). Indirect neutron measurements.
[d]Extrapolated using speed of sound $s=1000\pm200$ m/sec, based on experimental data near this density (Ref. 19).
[e]Stassis, Khatamian, and Kline (Ref. 18). Direct neutron measurements.

Solid helium is known to have a significant phonon linewidth. For small k, the phonon linewidth can be approximated to be $\gamma_k\cong0.2\omega_k$.[12,13] For a damped harmonic lattice,

$$A_{\rm damped}(k,\omega)=\frac{\hbar}{2m\omega_k}\left(\frac{\gamma_k}{(\omega-\omega_k)^2+\gamma_k^2/4}-\frac{\gamma_k}{(\omega+\omega_k)^2+\gamma_k^2/4}\right). \tag{20}$$

Integrating over ω, we find that for $T=0$,

$$A(k)=\frac{2\hbar}{m\omega_k}\tan^{-1}\left(\frac{2\omega_k}{\gamma_k}\right)\propto\frac{1}{\omega_k}, \tag{21}$$

which gives $\nu=1$. For $T>0$, Eq. (20) can be integrated numerically. As before, we find $\nu=2$ when $k_BT\gg\hbar\omega_k$ and $\nu=1$ when $k_BT\ll\hbar\omega_k$, with a crossover at $\hbar\omega_k\approx k_BT$, with width in $\hbar\omega_k/k_BT$ equal to that of the undamped harmonic lattice.

The width of the crossover region is defined in terms of the ratio $\hbar\omega_k/k_BT$ (see Fig. 2). The phonons excluded from the finite system have linear dispersion with an upper bound of $\omega_k=sk_c=2\pi s\rho^{1/3}/N^{1/3}$, where s is the speed of sound. By choosing typical values for temperature, density and sound speed, we can estimate the width of the crossover region as a function of the number of particles N. For example, if we assume the speed of sound is $s\cong4.0\times10^{13}$ Å/sec, we find that for temperature $T=20.0$ K and density ρ

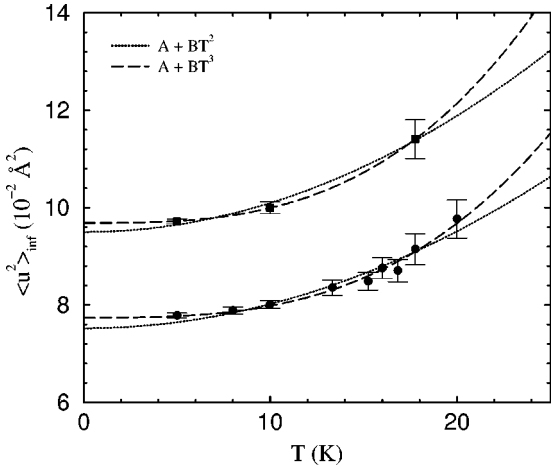

FIG. 3. Temperature dependence of $\langle u^2\rangle_\infty$, using the extrapolated values from Table I. Shown are values for fcc ^{4}He, $V_m = 10.98$ cm^3 (solid circles), and fcc ^{3}He, $V_m = 11.54$ cm^3 (solid squares).

$=0.055$ Å^{-3}, $N_{\text{crossover}} \sim 10^2$–$10^5$. A simple power law fit to system sizes in this range is inaccurate.

If we assume a harmonic spectrum, we can use Eq. (19) to write

$$\delta\langle u^2\rangle \propto \int_0^{k_c} dk\, k^2 A(k) \propto \int_0^{k_c} dk\, k \coth\left(\frac{\beta\hbar\omega_k}{2}\right)$$
$$\propto N^{-1/3}\left[1+\ln\left(\frac{1-\exp(-BN^{-1/3})}{BN^{-1/3}}\right)\right]$$
$$+\mathcal{O}(N^{-1}), \tag{22}$$

where $B \equiv 2\pi\beta\hbar s\rho^{1/3}$. The functional form of $\langle u^2\rangle$ can now be written as

$$\langle u^2\rangle = \langle u^2\rangle_\infty - AN^{-1/3}\left[1+\ln\left(\frac{1-\exp(-BN^{-1/3})}{BN^{-1/3}}\right)\right]. \tag{23}$$

The parameter B is not effectively constrained by the PIMC values of $\langle u^2\rangle$ versus N, and therefore cannot be accurately determined by fitting. Instead, by using physically reasonable values of B, we can use least-squares fitting (of A and $\langle u^2\rangle_\infty$) to extrapolate our PIMC data to the thermodynamic limit and get values for $\langle u^2\rangle_\infty$ (see Table I). The speed of sound s can be obtained from experimental measurements of isothermal compressibility κ_T,[14] using the relationship

$$s^2 = \frac{1}{\rho m \kappa_T}, \tag{24}$$

However, we obtained poor fits using the value of B obtained in this manner. The lack of self-consistency with physical parameters shows that the undamped harmonic lattice used to derive Eq. (23) is insufficient for describing the mean-squared displacement in solid helium. A larger range of B was required for reasonable fitting, both due to anisotropy in s and the approximations used in calculating the functional form Eq. (23). We were able to obtain reasonable fitting by using values of B which correspond to $s=4000$ ± 2000 m/sec, which is larger than experimental values by about a factor of 2 on average. For systems away from melting, the fitting was insensitive to the value of B, and the propagated error from B was on the same order of magnitude as the fitting error, in estimating $\langle u^2\rangle_\infty$. The reduced χ^2 for systems away from melting was typically between 0.1 and 1.0. For systems near melting, the fitting was much more sensitive to the estimated range of B, particularly the lower bound, and the error bar on $\langle u^2\rangle_\infty$ was completely determined by the uncertainty in B. The reduced χ^2 for these systems was usually between 5 and 10. A more accurate functional form, perhaps one which takes the phonon linewidth into account, would greatly improve the accuracy of extrapolating to the thermodynamic limit for these systems.

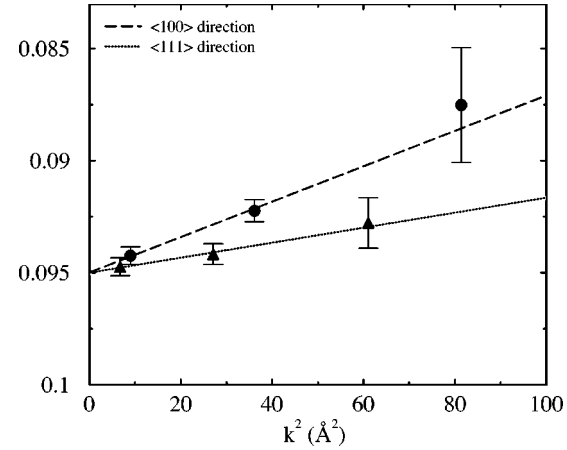

FIG. 4. $(1/k^2)\ln\{[S(k)-1]/(N-1)\}$ versus k^2 for fcc ^{4}He, $V_m = 10.98$ cm^3, $N=864$, $T=20.0$ K. The kurtosis κ is given by the slope, and agrees with direct calculations of $\langle u^4\rangle/\langle u^2\rangle^2-3$. In the $\langle 100\rangle$ direction (dashed line), the fitted kurtosis was 0.11 ± 0.03, while the direct value was 0.09 ± 0.03. In the $\langle 111\rangle$ direction (dotted line), the fitted kurtosis was 0.05 ± 0.03, while the direct value was 0.02 ± 0.03.

Our PIMC calculations agree with all direct scattering measurements of $\langle u^2\rangle$, when extrapolated to the thermodynamic limit. We are able to confirm both computational and experimental methods to an accuracy of 5% in the mean-squared displacement. Near melting, the accuracy of the PIMC values was considerably reduced, due to uncertainty in the functional form of the finite-size effects. PIMC values were generally higher than the indirect scattering measurements.[17] Because the indirect measurements assumed contributions from single-phonon processes only, this discrepancy gives evidence for the importance of multiphonon processes in solid helium.

IV. TEMPERATURE DEPENDENCE

Using Eq. (19), it is straightforward to show that the harmonic approximation predicts $\langle u^2\rangle_\infty$ to have temperature dependence of the form

$$\langle u^2\rangle_\infty = \langle u^2\rangle_\infty^{T=0} + CT^2. \tag{25}$$

However, our extrapolated values of $\langle u^2\rangle$ appear to fit to a T^3 power law, rather than T^2 for $5 \leqslant T \leqslant 20$ K (see Fig. 3). With less than a decade in temperature, it is difficult to draw any direct conclusions from this, although it may indicate

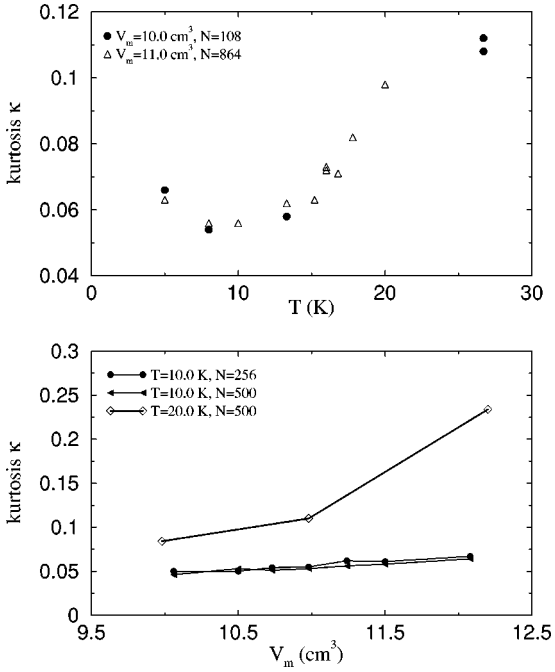

FIG. 5. Kurtosis κ vs molar volume V_m and temperature T, in the $\langle 100 \rangle$ direction, for fcc ^{4}He. The kurtosis is noticeably larger near the experimental melting line, but is otherwise independent of temperature and density.

that harmonic theory is insufficient to accurately describe solid helium, and that higher order terms dominate the temperature dependence.

V. NON-GAUSSIAN CORRECTIONS TO $\langle u^2 \rangle$

We have determined the deviation of the density from a Gaussian distribution by two methods. The first was fitting $\ln[S(k)]$ to a polynomial in k^2. As shown in Eq. (7), the linear term is $\langle u^2 \rangle$, the quadratic term is proportional to the kurtosis κ. We also directly calculated the kurtosis in the $\langle 111 \rangle$ and $\langle 100 \rangle$ directions, using Eq. (8). The kurtosis was found to be nonzero and anisotropic in the fcc solid helium systems we studied (see Fig. 4). The spherically averaged kurtosis $\bar{\kappa}$ at 10.98 cm^3 is 0.074(20). Shown in Fig. 5 are graphs with kurtosis in the $\langle 100 \rangle$ direction as a function of density and temperature. The kurtosis is roughly twice as large in systems near melting. Away from melting, the kurtosis appears to be independent of both temperature and density. We found that κ is independent of N, for values of $N \geqslant 500$. For smaller system sizes, the finite-size effects are large, but drop off quickly with increasing N. However, at the wave vectors $k \leqslant 9$ Å^{-1}, the effect of the kurtosis is only a few percent, making this term difficult to observe in scattering experiments.[13,15,16,18,20]

Vitiello *et al.*[21] have computed spherically averaged kurtoses of 0.051(5) and 0.042(5) at zero temperature using shadow wave functions, for molar volumes of 20.5 cm^3 and 18.3 cm^3. Using more accurate shadow wave functions, MacFarland *et al.*[10] computed a spherically averaged kurtosis of 0.042(6), for a molar volume of 18.3 cm^3. These values are consistent with the values computed here.

VI. CONCLUSIONS

PIMC simulations of the Debye-Waller factor in solid helium agree with experimental results to better than 5% accuracy, indicating that the assumed potential, the computational methods, and the experimental analysis are correct within the stated errors. We determined the first non-Gaussian contribution, a directionally dependent kurtosis. The finite-size effects were found to be in a crossover region between the classical and quantum scaling limits, and hence a power-law dependence was insufficient for extrapolation to the thermodynamic limit. The harmonic approximation gave an approximate functional form for $\langle u^2 \rangle$ which was used to extrapolate finite values to the thermodynamic limit. The extrapolated values agree with all available direct scattering measurements, although the extrapolation became more sensitive with increased proximity to the melting transition, with correspondingly larger uncertainties. Higher extrapolation accuracy could be obtained with a more accurate scaling form. The effective temperature dependence of $\langle u^2 \rangle$ appears to be closer to T^3, rather than the T^2 predicted by harmonic theory.

ACKNOWLEDGMENTS

The authors wish to thank R. O. Simmons, G. Baym, G. H. Bauer, and N. Goldenfeld for useful discussions. This research was carried out on the Origin 2000 at the National Center for Supercomputing Applications, and was supported by the NASA Microgravity Research Division, Fundamental Physics Program.

[1] H.R. Glyde, *Excitations in Liquid and Solid Helium* (Clarendon Press, Oxford, 1994).
[2] N.G. Van Kampen, *Stochastic Processes in Physics and Chemistry* (North-Holland, Amsterdam, 1992).
[3] D.M. Ceperley, Rev. Mod. Phys. **67**, 279 (1995).
[4] R.A. Aziz, A.R. Janzen, and M.R. Moldover, Phys. Rev. Lett. **74**, 1586 (1995).
[5] A.R. Janzen and R.A. Aziz, J. Chem. Phys. **107**, 914 (1997).
[6] T. Korona, H.L. Williams, R. Bukowski, B. Jeziorski, and K. Szalewicz, J. Chem. Phys. **106**, 5109 (1997).
[7] D.A. Young and B.J. Alder, J. Chem. Phys. **60**, 1254 (1974).
[8] R.C. Shulka, F. Boseglav, and J.C. Whybra, Phys. Status Solidi B **195**, 73 (1996).
[9] K.J. Runge and G.V. Chester, Phys. Rev. B **38**, 135 (1988).
[10] T. MacFarland, S.A. Vitiello, L. Reatto, G.V. Chester, and M.H. Kalos, Phys. Rev. B **50**, 13 577 (1994).
[11] G.D. Mahan, *Many-Particle Physics*, 2nd ed. (Plenum Press, New York, 1993), Chap. 3.
[12] J. Eckert, W. Thomlinson, and G. Shirane, Phys. Rev. B **16**, 1057 (1977).
[13] C. Seyfert, R.O. Simmons, H. Sinn, D.A. Arms, and E. Burkel, J. Phys.: Condens. Matter **11**, 3501 (1999).

[14] A. Driessen, E. van der Poll, and Isaac F. Silvera, Phys. Rev. B **33**, 3269 (1986).
[15] D.A. Arms, Ph.D. thesis, University of Illinois at Urbana-Champaign, 1999.
[16] C.T. Venkataraman, Ph.D. thesis, University of Illinois at Urbana-Champaign, 1996.
[17] W. Thomlinson, J. Eckert, and G. Shirane, Phys. Rev. B **18**, 1120 (1978).
[18] C. Stassis, D. Khatamian, and G.R. Kline, Solid State Commun. **25**, 531 (1978).
[19] T.O. Brun, S.K. Sinha, C.A. Swenson, and C.R. Tilford (unpublished).
[20] C.A. Burns and E.D. Isaacs, Phys. Rev. B **55**, 5767 (1997).
[21] S.A. Vitiello, K.J. Runge, G.V. Chester, and M.H. Kalos, Phys. Rev. B **42**, 228 (1990).